










Phosphorylation at the disordered N-end makes HuR accumulate and dimerize in the cytoplasm

Blanca Baños-Jaime ¹, Laura Corrales-Guerrero ^{1,*}, Gonzalo Pérez-Mejías ¹,
 Claudia M. Rejano-Gordillo ^{2,3,4}, Adrián Velázquez-Campoy ^{5,6,7},
 Luis Alfonso Martínez-Cruz ^{2,3}, María Luz Martínez-Chantar ^{2,3}, Miguel A. De la Rosa ¹ and
 Irene Díaz-Moreno ^{1,*}

¹Institute for Chemical Research (IIQ), Scientific Research Center “Isla de la Cartuja” (cicCartuja), University of Seville - CSIC, Seville 41092, Spain

²Centre for Biomedical Research Network of Hepatic and Digestive Diseases (CIBERehd), Madrid 28029, Spain

³Liver Disease Lab, BRTA CIC bioGUNE, Derio 48160 Bizkaia, Spain

⁴Department of Biochemistry and Molecular Biology, Faculty of Sciences, University of Extremadura; University Institute of Biosanitary Research of Extremadura (INUBE), Badajoz 06071, Spain

⁵Institute for Biocomputation and Physic of Complex Systems (BIFI), Joint Unit GBSC-CSIC-BIFI, University of Zaragoza, Zaragoza 50018, Spain

⁶Departament of Biochemistry and Molecular and Cellular Biology, University of Zaragoza, Zaragoza 50009, Spain

⁷Institute for Health Research of Aragón (IIS Aragón), Zaragoza 50009, Spain

*To whom correspondence should be addressed. Tel: +34 954489513; Email: idadmoreno@us.es

Correspondence may also be addressed to L. Corrales-Guerrero. Tel: +34 954489640; Email: laucorge@us.es

Present addresses:

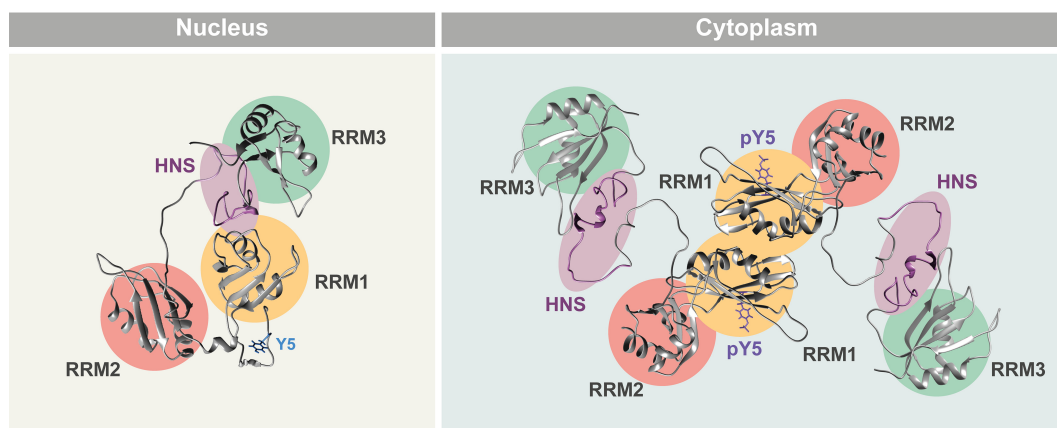
L. Corrales-Guerrero, Institute of Plant Biochemistry and Photosynthesis (IBVF), Scientific Research Center “Isla de la Cartuja” (cicCartuja), University of Seville - CSIC, Seville 41092, Spain.

G. Pérez-Mejías, German Center for Neurodegenerative Diseases (DZNE), Göttingen 35075, Germany.

Abstract

Human antigen R (HuR) is an RNA binding protein mainly involved in maintaining the stability and controlling the translation of mRNAs, critical for immune response, cell survival, proliferation and apoptosis. Although HuR is a nuclear protein, its mRNA translational-related function occurs at the cytoplasm, where the oligomeric form of HuR is more abundant. However, the regulation of nucleo-cytoplasmic transport of HuR and its connection with protein oligomerization remain unclear. In this work, we describe the phosphorylation of Tyr5 as a new hallmark for HuR activation. Our biophysical, structural and computational assays using phosphorylated and phosphomimetic HuR proteins demonstrate that phosphorylation of Tyr5 at the disordered N-end stretch induces global changes on HuR dynamics and conformation, modifying the solvent accessible surface of the HuR nucleo-cytoplasmic shuttling (HNS) sequence and releasing regions implicated in HuR dimerization. These findings explain the preferential cytoplasmic accumulation of phosphorylated HuR in HeLa cells, aiding to comprehend the mechanisms underlying HuR nucleus-cytoplasm shuttling and its later dimerization, both of which are relevant in HuR-related pathogenesis.

Graphical abstract



Received: October 24, 2023. Revised: May 30, 2024. Editorial Decision: June 11, 2024. Accepted: July 2, 2024

© The Author(s) 2024. Published by Oxford University Press on behalf of Nucleic Acids Research.

This is an Open Access article distributed under the terms of the Creative Commons Attribution-NonCommercial License

(<https://creativecommons.org/licenses/by-nc/4.0/>), which permits non-commercial re-use, distribution, and reproduction in any medium, provided the original work is properly cited. For commercial re-use, please contact reprints@oup.com for reprints and translation rights for reprints. All other permissions can be obtained through our RightsLink service via the Permissions link on the article page on our site—for further information please contact journals.permissions@oup.com.

Introduction

Posttranslational modifications (PTMs) consist in the covalent addition of functional groups or biomolecules to proteins, as well as other chemical changes of their constituent amino acids and even the cleavage of peptide bonds, during or after their synthesis. PTMs play a critical regulatory role in cell metabolism, as they can modify the charge and structure of proteins, thus altering their function, stabilization and localization. The RNA binding protein (RBP) Human antigen R (HuR) is particularly regulated by PTMs (1,2). HuR, also known as ELAV-like protein 1 (ELAVL1), is involved in mRNA stabilization and degradation (3–5). HuR is composed of three RNA recognition motifs (RRM), and each of them contains two ribonucleoprotein domains (RNP). A disordered region of 20 residues length precedes the RRM1, which forms a tandem structure with the RRM2. A 60-residue disordered region, the so-called hinge region, connects RRM2 and RRM3 (6–8). Although HuR is a predominantly nuclear protein, the hinge region contains the HuR nucleo-cytoplasmic shuttling (HNS) sequence (residues 205–237), which is responsible for the HuR transport between nucleus and cytoplasm (9). The HNS sequence is not homologous to canonical Nuclear Localization Signals (NLS) or Nuclear Export Signals (NES). However, it is known that the essential residues in maintaining HuR at the nucleus are located at the beginning of the HNS sequence (R205, R206 and F207, and probably H212, H213, R217 and R219) (9,10). In fact, cleavage of HuR at D226 by caspases 3 and 7 at the cytoplasm generates two HuR cleavage products (CP). HuR-CP1, but not HuR-CP2, interacts with transportin 2 (Trn2) and returns to the cell nucleus (11–13).

HuR is susceptible to numerous modifications, but the most common is phosphorylation (1). As a general rule, changes near the RRM1s usually alter HuR affinity towards nucleic acids, whereas modifications on the hinge region tend to modulate HuR localization. For instance, protein kinase C δ (PKC δ) phosphorylates HuR on S318, at the RRM3 domain, improving HuR-mRNA binding ability, while the phosphorylation on S221, at the hinge region, by protein kinase C α (PKC α) promotes its translocation from the nucleus to the cytoplasm (14,15). Tyrosine phosphorylation has also been described to regulate HuR function. Indeed, phosphorylation by Janus Kinase 3 (JAK3) at HuR Y200, at the beginning of the hinge region, diminishes HuR-mRNA affinity. Upon stress conditions, a cytoplasmic fraction of HuR is relocated to stress granules (SGs), but phosphorylation on Y200 excludes HuR from these membraneless organelles (16). Y200 and three more tyrosine residues (Y5, Y95 and Y109) were previously suggested as consensus sites for Abl1 and Src kinases, although no experimental evidence has been provided. Interestingly, the non-phosphorylatable HuR with the four Tyr-by-Phe substitutions, reduced protein accumulation on the centrosomes, which was proposed to be regulated by HuR phosphorylation (17).

The accumulation of HuR at the cytoplasm is typically associated with conditions that require high mRNA regulation and HuR activity, such as stress stimuli or cell proliferation and differentiation (5,14,18). By modulating the synthesis of proinflammatory mediators, HuR plays a decisive role in stress response, infections and other pathophysiological processes, especially cancer development, where HuR expression and activity increase (7,10,14,19–21). Indeed, elevated cytoplasmic localization of HuR is related to its tumorigenic po-

tential, which has been correlated with poor prognosis of several types of cancer as breast, esophageal or lung carcinoma (reviewed in (22)). The activation of HuR is also related to its oligomerization (23). In fact, the HuR inhibitors dehydromutacin and MS-444 prevent HuR-RNA recognition, as well as HuR dimerization and its translocation to the cytoplasm (24).

In this study, we identify Y5 as a new phosphorylation site of HuR and explore the structure, dynamics and function of Y5 phosphorylation by combining biophysical and cellular techniques. Although Y5 is located at the disordered N-terminal stretch of HuR, we show that its phosphorylation increases the dynamic behaviour of the hinge region, modifying the HNS sequence solvent exposure, and thus promoting the nucleo-cytoplasmic shuttling. In addition, the increased dynamics of disordered stretches improves the availability of key RRM1 residues involved in HuR dimerization. Thus, Y5 phosphorylation represents a novel regulation mode for HuR activation that leads to higher oligomeric protein levels at the cytoplasm.

Materials and methods

A more detailed version of the Methods can be found in Supplementary Methods.

Cell cultures and plasmid construction

HeLa and Jurkat cell lines were cultured in Dulbecco's modified Eagle's medium (DMEM) (D5796-500mL, Sigma-Aldrich) and RPMI1640 (R8758-500mL, Sigma-Aldrich), respectively, at 37°C in a humidified atmosphere of 5% CO₂. Both media were supplemented with 10% heat-inactivated fetal bovine serum (FBS) (P30-3306, PAN-Biotech), 2 mM L-glutamine (G7513-100ML, Sigma-Aldrich), 100 U/ml streptomycin and 100 μ g/ml penicillin (P433-100ML, Sigma-Aldrich). SGs formation was induced with 250 μ M sodium-arsenite (S7400-100G, Sigma-Aldrich) treatment for 45 min. When indicated, cells were treated with 10 μ M doxorubicin (D1515-10MG, Merck) for 4 h.

The plasmids and oligonucleotides in this work are listed in [Supplementary Tables S1](#) and [S2](#). All newly constructed plasmids were verified by DNA sequencing. Detailed information about plasmid construction can be found in [Supplementary Methods](#).

Western blots analyses

HeLa and Jurkat cells were lysed in TR3 buffer (3% SDS, 10% glycerol, 10 mM Na₂HPO₄) or RIPA buffer (1.6 mM Na₂HPO₄, 8.4 mM NaH₂PO₄, 0.1 M NaCl, 0.1% SDS, 0.1% Triton X-100), supplemented with 2.5 mg/ml sodium-deoxycholate (D6750-25G, Sigma-Aldrich), complete protease inhibitor cocktail (05056489001, Roche) and 1 mM sodium orthovanadate (A2196,0005, AppliChem) or phosphatase inhibitor cocktails (P2850, Sigma-Aldrich); and then centrifuged at 20000 \times g for 15 min. Protein content was measured using the DC Protein Assay (5000116, Bio-Rad Laboratories) with bovine serum albumin (BSA) (23210, Thermo-Scientific) as a standard, and 20 or 60 μ g protein was loaded for each lane.

To detect HuR oligomeric species by western blotting, HeLa cells were seeded in 6-well plates and transfected with plasmids carrying V5-tagged HuR WT or HuR Y5F ([Supplementary Table S1](#)), using Lipofectamine 3000 trans-

fection reagent (L3000001, Invitrogen), as stated in the manufacturer's instructions. After 24 h, cells were lysed in 50 mM BisTris pH 7.2, 50 mM NaCl, 10% w/v Glycerol, 0.001% Ponceau S and 1% digitonin, supplemented with 2.5 mg/ml sodium-deoxycholate (D6750-25G, Sigma-Aldrich), complete protease inhibitor cocktail (05056489001, Roche) and 1 mM sodium orthovanadate (A2196,0005, AppliChem). For samples in reduced and denatured conditions, the buffer was supplemented with β -mercaptoethanol and preheated at 95°C for 5 min before gel loading. However, for samples in non-reduced and non-denatured conditions, β -mercaptoethanol was not added and the preheating step was omitted as described before (23). Then, samples were separated by SDS-PAGE (8%, 12% or 15% acrylamide) and transferred onto polyvinylidene difluoride (PVDF) membranes. Membranes were blocked with 5% BSA (A3294, Sigma-Aldrich) in Tris-Base buffered saline (TBS)-0.1% Tween-20 for 1 h at room temperature.

For HuR and HuR pY5 detection, primary rabbit anti-HuR pY5 (made by ProteoGenix against the peptide CM-SNG(pY)EDHMAED; [Supplementary Figure S1A, B](#)) and mouse anti-HuR (WH0001994M2, Sigma-Aldrich) were used. For V5-tag detection, membranes were incubated overnight at 4°C with V5-tag primary antibody (1:1000) (R960-25, Invitrogen). The immunoreactive bands were detected using Immobilon Western Chemiluminescent HRP Substrate (WBKLS0500, Millipore). The chemiluminescent signal from immunoreactive proteins was detected in the ImageQuant LAS 4000 imaging system (GE Healthcare). Protein bands were quantified by densitometric analysis using ImageLab v6.1 (BioRad) or the open source image processing program ImageJ software and normalized to tubulin housekeeping protein expression (25).

To test the specificity of the antibody against HuR pY5, 385 μ g/ml HuR proteins were incubated with 20 μ g/ml kinase domain of JAK3 (provided by Prof. Patrick Celie at the Netherlands Cancer Institute), a kinase previously found to phosphorylate HuR at tyrosine residues (26), and 1.5 mM ATP for 20 h at 4°C in 20 mM HEPES, pH 7.4, supplemented with 1 mM $MgCl_2$ and 1 mM $MnCl_2$. Dephosphorylation was performed with 3 U/ml alkaline phosphatase (P7640, Sigma-Aldrich) incubated for 30 min at 37°C.

Immunofluorescence

HeLa cells were grown for 24 h on 20 mm glass coverslips, in 24-well plates containing 500 μ l of supplemented DMEM. When indicated, HeLa cells were transfected with plasmids carrying V5-tagged HuR WT or HuR Y5F ([Supplementary Table S1](#)), using DharmaFECT transfection reagent (T-2001-03, Horizon Discovery) and Opti-MEM I reduced serum medium (31985070, Gibco), as stated in the manufacturer's instructions. After 24 h, cells were washed with phosphate buffer saline (PBS) (P4417-50TAB, Sigma-Aldrich), then fixed with 4% paraformaldehyde (w/v) (F8775-500, Sigma-Aldrich), prepared in PBS, for 15 or 20 min at room temperature (RT). Afterward, cells were washed three times in PBS and permeabilized with 0.2% Triton X-100 or 0.2% BSA-0.1% Triton X-100, prepared in PBS, for 10 min at RT. After blocking with 2% or 3% BSA, prepared in PBS, for 30 min at RT, cells were incubated overnight at 4°C with rabbit anti-HuR pY5 (1:150), prepared in blocking buffer. Coverslips were washed with PBS and incubated for 1 h at RT with mouse anti-HuR (1:500), prepared in block-

ing buffer. Transfected HeLa cells were incubated overnight at 4°C with mouse anti-V5-tag (1:100) prepared in blocking buffer. Then, coverslips were washed three times with PBS and probed with the secondary antirabbit IgG-FITC antibody (1:500) and antimouse Alexa Fluor 568 (1:500), or with secondary Alexa Fluor 488 (1:500) prepared in blocking buffer for 1 h at RT. Nuclei were stained by 10 min RT incubation with 200 μ g/ml Hoechst dye (Sigma-Aldrich) or Fluoroshield with DAPI (F6057, Sigma-Aldrich). Cells were washed with PBS before immersed in pure ethanol for 2 min, dried for a few minutes, mounted using *n*-propyl gallate (02370-100G, Sigma-Aldrich) and sealed with nail polish.

Fluorescence was monitored with an Olympus FLUOVIEW FV3000 confocal laser-scanning microscope equipped with an UPlanApo 40 \times /1.4 NA oil immersion objective, or with a Leica SP8 Laser Confocal Microscope equipped with 63 \times HC PL APO/1.4 NA oil immersion objective. Samples were excited with 405, 488 and 561 nm for nuclei Hoechst dye, HuR pY5 and total HuR respectively. Fluorescence emission was detected between 359–461, 499–520 and 579–603 nm.

Fluorescence quantification of endogenous HuR and HuR pY5 or exogenous V5-tagged HuR WT and HuR Y5F in HeLa cells was calculated as the percentage of the total fluorescence intensity in the nucleus with respect to that in the whole cell or in SGs with respect to that in the whole cell or in the cytoplasm. Fluorescence intensity was quantified using ImageJ and data were analysed with Origin 2019b (OriginLab). Control samples containing secondary, but not primary antibodies, were used to set fluorescence levels to zero. Background fluorescence was extracted from cellular fluorescence in each image prior quantification.

Subcellular fractionation

Separation of 3×10^6 HeLa cell extracts into cytosol and nucleus fractions was performed with a ProteoExtract Subcellular Proteome Extraction Kit (539790, Calbiochem), according to the manufacturer's indications. Purity of subcellular fractions was verified by western blot analysis, using anti- α -tubulin (T9026, Sigma-Aldrich) and anti-histone H3 (ab1791, Abcam) antibodies for specific detection of cytosol and nucleus, respectively.

Protein expression and purification

Unlabeled HuR₂₋₉₉ and HuR₂₋₁₈₉ proteins were expressed in *Escherichia coli* BL21 (DE3) cells (70235, Novagen) in Luria Bertani (LB) medium supplemented with 100 μ g/ml ampicillin for 20 h at 30°C and 150 rpm after induction with 1 mM isopropyl- β -D-thiogalactopyranoside (IPTG) (R3679, iNtRON Biotechnology). Incorporation of pCMF was accomplished as previously described (27). Briefly, culture was incubated at 37°C at 150 rpm in minimal medium M9 supplemented with 100 μ g/ml ampicillin and 20 μ g/ml chloramphenicol. Pre-induction of the pre-culture with 0.02% arabinose (A3256-25G, Sigma-Aldrich) is necessary to ensure the presence of the unnatural tRNA/aaRS pair. Protein expression was induced at an optical density (OD₆₀₀) of 0.6 with 0.02% arabinose and 1 mM IPTG; pCMF was added after induction at a final concentration of 1 mM.

¹⁵N- and ¹⁵N-¹³C labeled proteins were expressed in minimal medium M9 supplemented with ¹⁵NH₄Cl (1 g/l) or ¹⁵NH₄Cl (1 g/l) and ¹³C₆-glucose (4 g/l), respectively.

Full-length HuR proteins were expressed in *E. coli* BL21 (DE3) cells in LB media supplemented with 100 µg/ml ampicillin for 60 h at 12 °C and 150 rpm after induction with 0.5 mM IPTG.

To purify HuR₂₋₁₈₉ and HuR₂₋₉₉ and its mutant derivatives, cells were collected by centrifugation (4200 × g for 10 min), and then resuspended in lysis buffer (20 mM Tris-HCl, pH 8.0, 800 mM NaCl and 10 mM imidazole), supplemented with 1 mM phenylmethylsulfonyl fluoride (PMSF) (93482-50ML-F, Sigma-Aldrich), 0.02 mg/ml DNase (10104159001, Roche) and 0.2 mg/ml lysozyme (89833, ThermoScientific). Cells were ruptured by sonication (cycles of 10 s at 35% of amplitude, 20 s of rest, 4 min total time, on ice), and cell debris was removed by centrifugation at 20000 × g at 4°C for 60 min. For proteins purification, cell lysates were incubated with HisPur™ Ni-NTA resin (88222, ThermoScientific), previously equilibrated with lysis buffer, and eluted with buffer 20 mM Tris-HCl pH 8, supplemented with 200 mM NaCl, using a non-continuous imidazole gradient (10–300 mM imidazole). Fractions containing the protein of interest were pooled and dialyzed at 4°C in three steps against 5 l of buffer 20 mM HEPES pH 7.4, buffer 20 mM citrate pH 5.5, 100 mM NaCl or buffer 20 mM sodium-phosphate pH 7.

For purification of full-length HuR proteins, a second purification step was performed by loading the fractions containing the protein of interest onto a 5 ml MBPTrap affinity column (28-9187-79, Cytiva). The column was washed with buffer 20 mM Tris-HCl pH 7.4 supplemented with 1 mM ethylenediaminetetraacetic acid (EDTA), 1 mM dithiothreitol (DTT) and 1 mM PMSF, and protein was eluted in one step with the same buffer containing 25 mM maltose. Fractions containing the protein of interest were pooled and dialyzed at 4°C in two steps against 5 l of buffer 20 mM HEPES pH 7.4 or buffer 20 mM citrate pH 5.5, 100 mM NaCl.

Proteins were used freshly purified. Protein concentrations were determined before every experiment with the Bradford assay, using the Bio-Rad Protein Assay Dye Reagent (5000006, Bio-Rad) with BSA (23210, ThermoScientific) as a standard.

Molecular dynamics simulations

The initial structures of HuR₂₋₉₉ were based on the nuclear magnetic resonance (NMR) structure of HuR RRM1 (PDB ID: 5SZW) (28). To trace the unstructured linker between domains RRM2 and RRM3, the structural model of HuR RRM2-RRM3 was built with MODELLER (29) using as templates the X-ray structures of PDB entries 4ED5 (6) and 6GD3 (8). The initial structure of HuR₁₋₃₂₆ was created from the resulting structure of HuR RRM2-RRM3, the NMR structure of HuR RRM1 and the X-ray structure of HuR RRM1 and RRM2 (PDB ID: 4EGL) (6). All mutants and phosphorylated models were built using the wild-type proteins as templates. The force field parameters for phosphorylated tyrosine (30) and unnatural amino acid pCMF (31) were used to generate the topology and coordinate files required for the simulation, with the TLEAP module of AMBER (32).

Molecular dynamics (MD) simulations were performed using the OpenMM (33) software in CUDA platform with AMBER 14SB force field (34) and particle mesh Ewald electrostatics with an Ewald summation cut-off of 10 Å. For each simulation, the system was neutralized with sodium and chlorine counter-ions according to the total charge of the pro-

tein and solvated with optimal-3-charge, 4-point rigid water model water molecule (35). The whole system was subjected to 2500 steps of energy minimization at 298 K. Langevin thermostat was used to control the temperature with a friction coefficient of 1 ps⁻¹ and a step size of 0.002 ps. Systems were subjected to MD simulations of 1 µs for HuR₂₋₉₉ and 300 ns for HuR₁₋₃₂₆. For the trajectory analysis, the CPPTRAJ module of AMBER was used (36). Contact maps were created with Contact Map Explorer tool of MDTraj library (37). Cut-off distance was set at 0.45 nm for HuR₂₋₉₉ and 0.7 nm for HuR₁₋₃₂₆. Solvent-accessible surface areas (SASA) were calculated with SASA Calculation tool of MDTraj library.

Nuclear magnetic resonance spectroscopy

For nucleic magnetic resonance (NMR) 2D ¹H-¹⁵N-HSQC spectrum assignment, we performed 3D ¹H-¹⁵N-¹³C-HNCACB and 3D ¹H-¹⁵N-TOCSY-HSQC experiments. For 2D ¹H-¹⁵N-HISQC spectra assignment, we performed 2D ¹H-¹⁵N-(H2C)N(CCH) and 2D ¹H-¹⁵N-H2CN experiments. All assignment spectra were recorded on a 600 MHz Bruker Avance-III spectrometer equipped with a cryoprobe (BMRB accession number for ¹⁵N-¹³C-labelled HuR₂₋₉₉ Y5pCMF: 52173). Sample contained 690 µM of ¹⁵N-¹³C-labelled HuR₂₋₉₉ Y5pCMF in citrate buffer (20 mM sodium-citrate pH 5.5, 100 mM NaCl, 5% D₂O) supplemented with 5 mM TCEP.

2D ¹H-¹⁵N-HSQC spectra of 300 µM HuR₂₋₉₉ and 200 µM HuR₂₋₁₈₉ samples were recorded in citrate buffer supplemented with 2 mM TCEP, on a 500 MHz Bruker Avance-III spectrometer equipped with a cryoprobe.

Solvent paramagnetic relaxation enhancement (sPRE)-NMR experiments were performed on a 500 MHz Bruker Avance-III spectrometer equipped with a cryoprobe. Samples contained 200 µM of ¹⁵N-labelled HuR₂₋₉₉ wild-type or Y5pCMF mutant in citrate buffer. Carboxy-PROXYL and carbamoyl-PROXYL probes were added at 5 mM for negative and neutral paramagnetic experiments, respectively. For diamagnetic experiments, samples were measured with no probe. Rates for negative and neutral probes were calculated as previously described (38) using Origin 2019b.

NMR titration of 100 µM HuR₂₋₉₉ wild-type and Y5pCMF samples with 5'-ATTTTTA-3' oligonucleotide, were performed as independent samples in citrate buffer supplemented with 2 mM TCEP, on a 700 MHz Bruker Avance-III spectrometer equipped with a cryoprobe. Chemical-shift perturbations (ΔCSP) for residues Leu22, Ala57 and Arg97, calculated as previously described (39), were used to estimate K_D. This analysis was performed with Origin 2019b (OriginLab).

2D ¹H-¹⁵N-HSQC, 3D ¹H-¹⁵N-¹³C-HNCACB and 3D ¹H-¹⁵N-TOCSY-HSQC experiments were performed at 298 K. 2D ¹H-¹⁵N-HISQC experiment was performed at 278 K to enhance NH₃⁺ lysine side chain detection. 2D ¹H-¹⁵N-(H2C)N(CCH) experiment was performed at 308 K to improve ¹³C-¹³C Hartmann-Hahn cross polarization. Non-uniform spectral sampling (NUS) was used to collect the data in 3D experiments.

The experimental data were processed using NMRPipe or Bruker TopSpin NMR 4.1.1 software (Bruker). CSPs were analysed with NMRFAM-Sparky NMR assignment tool (40) and Origin 2019b, and PRE-NMR data, with Origin 2019b. Protein structures were visualized using UCSF Chimera software (41).

Isothermal titration calorimetry

Isothermal titration calorimetry (ITC) dilution experiments of HuR₂₋₉₉ wild-type and HuR₂₋₉₉ Y5pCMF were performed using a Nano ITC Standard Volume instrument (TA Instruments, USA). Dilution assays consisted of 25 or 20 successive injections of 2 or 2.5 μ l, from a 700 μ M protein stock into the sample cell, containing the protein buffer.

ITC titration experiments of HuR₂₋₉₉ wild-type or HuR₂₋₉₉ Y5pCMF with 5'-ATTTTTA-3' oligonucleotide were performed using a Nano ITC Low Volume instrument (TA Instruments, USA). Titration experiments of HuR₂₋₉₉ with DNA consisted of 25 successive 2 μ l-injections, from a stock of 1.6 mM 5'-ATTTTTA-3' oligo into the sample cell, containing 250 μ M of HuR₂₋₉₉ wild-type or Y5pCMF mutant.

The reference cells were filled with distilled water. All ITC assays were performed at 20 mM sodium-citrate pH 5.5 supplemented with 100 mM NaCl and 1 mM TCEP, at 25°C. Homogeneous mixing was achieved by maintaining the stirring speed at 300 rpm. Data were processed and analysed using NanoAnalyze software (TA Instruments) and Origin 2019b (OriginLab).

Biolayer interferometry

Biolayer interferometry (BLI) analyses were performed on the Octet RED 96e platform (FortéBio) using Streptavidin Biosensors (SA) (FortéBio). The biosensors were hydrated in a 96-well black plate for 10 min with BLI buffer containing 20 mM HEPES pH 7.4, 100 mM NaCl, 5 mM TCEP for full length HuR wild-type and Y5pCMF mutant; and 20 mM citrate pH 5.5, 100 mM NaCl, 5 mM TCEP for HuR₂₋₉₉ wild-type or Y5pCMF mutant. Both BLI buffers were supplemented with 0.01% Triton X-100 and 0.01% rabbit serum albumin (RSA) to reduce non-specific binding to the biosensor. The biosensors were incubated with 2 μ M 5'-biotinylated single-stranded DNA oligonucleotide (5'-ATTTTTA-3' or 5'-ATTTTATTTTATTTT-3') (Sigma-Aldrich) diluted in BLI buffer. After the association step, the biosensors were transferred into the corresponding buffer to monitor the dissociation of protein-DNA complexes. The experimental data were processed with Data Analysis HT 12.0 software (FortéBio) and analysed with Origin 2019b.

Results

Y5 phosphorylation mediates HuR nucleo-cytoplasmic shuttling

Although phosphorylation on HuR Y5 had previously been detected by phosphoproteomic analyses, its presence in cells was not experimentally confirmed (17,42,43). Here, we used a custom-made antibody against a synthetic peptide containing the first 12 residues of HuR including phosphorylated Y5 (pY5). First, we assessed its specificity by examining its interaction with both wild-type and non-phosphorylatable variants of the HuR protein (Supplementary Figure S1A–D). Next, we tested whether HuR phosphorylated at Y5 (HuR pY5) can be found in cancer cell models as HeLa and Jurkat cells. As shown in Figure 1A, western blots revealed that both cell types did contain HuR pY5.

Afterwards, we studied the compartment localization of HuR pY5 in HeLa cells by immunofluorescence assays. In agreement with former reports (18), our fluorescence quan-

tification analysis revealed that HuR is a predominantly nuclear protein, with $76.1 \pm 7.5\%$ of total HuR being detected inside the nucleus. Surprisingly, phosphorylated pY5 protein was mainly cytoplasmic, with only $29.1 \pm 9.6\%$ of HuR pY5 retained at the nucleus (Figure 1B and Supplementary Figure S1E).

As many other RBPs, HuR associates with SGs under certain conditions, in order to regulate the fate of target RNAs as a part of the cell stress response (16,44,45). Indeed, phosphorylation of Y200 by JAK3 kinase inhibits the recruitment of HuR into SGs (16). For that reason, similar immunofluorescence experiments were performed to test whether Y5 phosphorylation affects HuR localization at SGs upon arsenite treatment. HuR pY5 nucleo-cytoplasmic distribution appeared to be independent from the stress response, exhibiting a very similar distribution to the one found under homeostatic conditions (Figure 1B and Supplementary Figure S1E). When comparing the fluorescence intensities of HuR and HuR pY5 in SGs over the total fluorescence of the cell, HuR pY5 presented an increased tendency to concentrate in SGs in comparison to total HuR (Supplementary Figure S1F). However, no differences were found between total HuR and HuR pY5 concentrated in SGs from the total cytoplasmic population (Figure 1C), indicating that the concentration in SGs of HuR pY5 is a consequence from the predominant cytoplasmic distribution rather than a specific effect of stress. Therefore, our results showed that Y5 phosphorylation regulates HuR nucleo-cytoplasmic shuttling without specifically affecting recruitment into SGs in HeLa cells.

Previously, it was shown that HuR travels to the cytoplasm upon doxorubicin treatment, which elicits the DNA damage response, in a phosphorylation-dependent manner (46). Therefore, we analysed the effect of doxorubicin on Y5-phosphorylation and localization of HuR by cell fractionation. As shown before, the cytoplasmic HuR population increased from 15% to 38% after the treatment with doxorubicin, while the total amount of HuR remained unchanged (after doxorubicin treatment the amount of HuR was 1.0 ± 0.3 -fold the amount under control conditions) (Figure 1D and E). Surprisingly, the rate of Y5-phosphorylated/total protein increased considerably after the addition of the drug (Figure 1F). To confirm the role of Y5 phosphorylation after doxorubicin treatment, we transfected HeLa cells with plasmids bearing V5-tagged HuR WT or a non-phosphorylatable version (HuR Y5F mutant), and detected their cellular location by immunofluorescence experiments using a V5-antibody (Figure 1G). Both WT and Y5F HuR versions remained nuclear under control conditions, although the non-phosphorylatable version Y5F presented a localization slightly more nuclear than the WT, presumably due to basal Y5 phosphorylation in the WT protein in HeLa cells. Thus, the average percentage of nuclear Y5F mutant (72.1%) was 6.2% higher than that for the WT version (65.9%). After doxorubicin treatment, HuR shuttled to the cytoplasm. As expected, difference between the average percentages of nuclear WT and Y5F versions were significant in this condition, increasing 12.6% (46.8% for HuR Y5F versus 34.2% for HuR WT) in agreement with a higher population of phosphorylated protein in WT HuR after doxorubicin treatment. These results suggest a physiological role of Y5 phosphorylation in the shuttling of HuR to the cytoplasm in response to DNA damage.

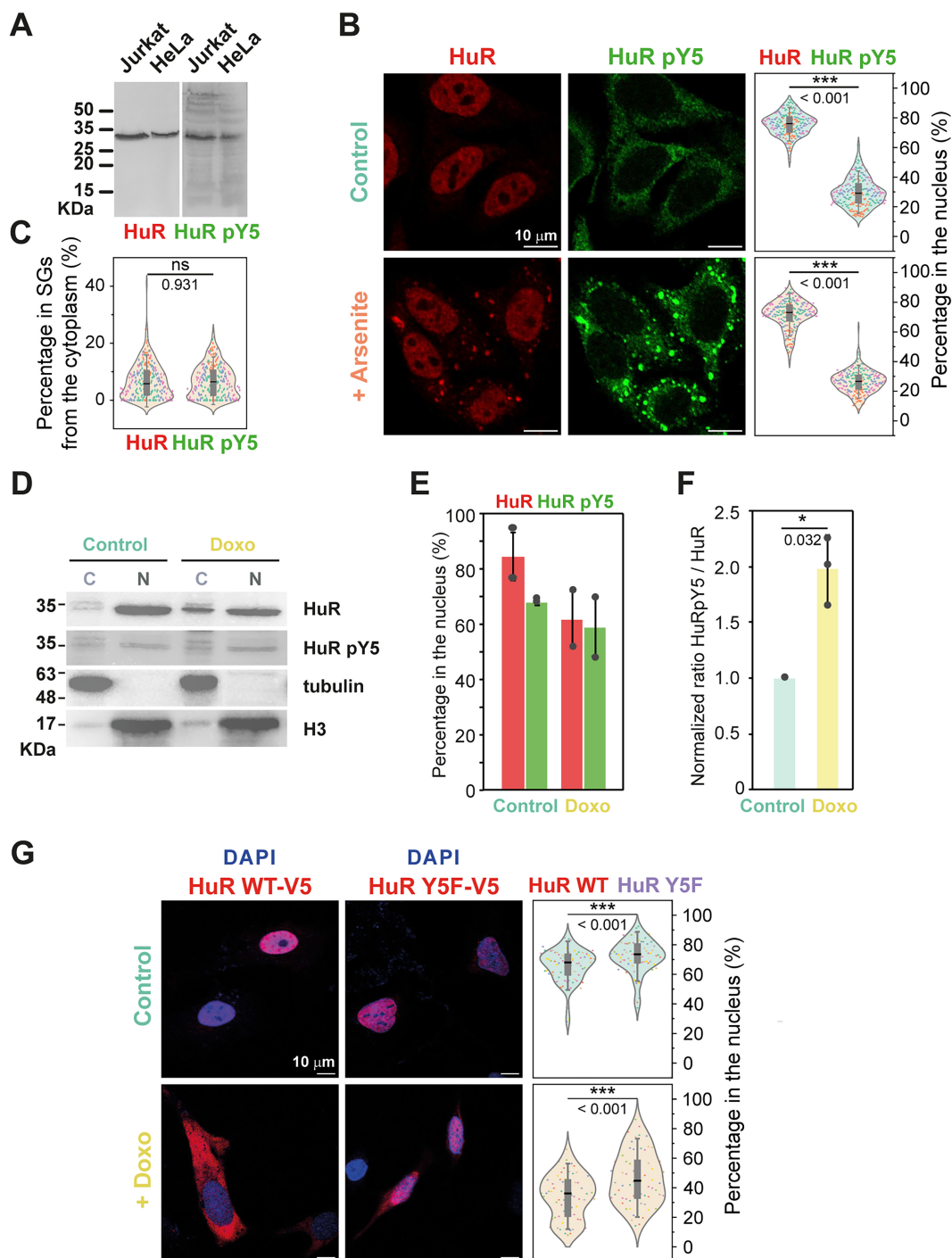


Figure 1. HuR Y5 phosphorylation causes HuR cytoplasmic accumulation. **(A)** Western blot analysis confirming HuR phosphorylation at Y5 in 10^6 Jurkat and HeLa cells by using anti-HuR and anti-HuR pY5 antibodies. **(B)** Immunofluorescence analysis of endogenous total HuR (red) and HuR pY5 (green) in HeLa cells under basal conditions (Control) and upon 45 min of 250 μ M arsenite treatment. Contrast and bright were adjusted equally in both conditions only for illustration purposes. *Right panels* show the results of fluorescence quantification of total HuR and HuR pY5 inside of the cell nuclei. For basal and stress conditions, 227 and 231 cells were quantified, respectively. Rotated kernel density plots are given for each dataset to show their distribution. Boxes indicate percentiles 25 and 75. Black lines indicate the median values, and whiskers indicate 1.5 times standard deviation values. The significance of differences was tested using the Student's *t* test. **(C)** Fluorescence quantification analysis of total HuR and HuR pY5 in stress granules from the total fluorescence intensity in the cytoplasm upon arsenite treatment, represented as in **(B)**. **(D)** 3×10^6 HeLa cells were incubated in the presence or absence of 10 μ M doxorubicin for 4 h. After that, cytoplasmic (C) and nuclear (N) fractions were submitted to Western blot using anti-HuR or anti-HuR pY5 antibodies. Tubulin and Histone H3 were used as cytoplasmic and nuclear markers, respectively. **(E)** Quantification of the percentage of the protein detected in the nucleus for anti-HuR or anti-HuR pY5 antibodies from **(D)**. Intensities from discrete bands were normalized against tubulin intensity for each condition. The average of 2 experiments is shown. Whiskers indicate standard deviation values. **(F)** Quantification of the ratio HuR pY5 over total HuR in each condition. The average of 3 experiments is shown. The significance of differences was tested using the Student's *t* test. Whiskers indicate standard deviation values. **(G)** Immunofluorescence analysis of wild-type or Y5F mutant versions of HuR-V5 (red) in HeLa cells. Nuclei (DAPI signal) are shown in blue. Cells were incubated in the presence or absence of 10 μ M doxorubicin for 4 h. *Right panels* show the results of fluorescence quantification of the nucleocytoplasmic distribution of 75 cells of each condition, represented as in **(B)**.

Y5 phosphorylation increases the dynamics of HuR disordered regions

To understand the changes observed *in cell*, we analysed the effect of Y5 phosphorylation on HuR structure by studying its behaviour *in vitro*. First of all, we constructed a truncated version, HuR₂₋₉₉, containing the disordered N-end and the first RNA-recognition domain (RRM1) of HuR (Supplementary Figure S2A). We demonstrated the independence of HuR RRM1 upon the tandem domain RRM1,2 by comparing the constructions HuR₂₋₉₉ and HuR₂₋₁₈₉ (which contains HuR RRM1 and RRM2; Supplementary Figure S2B). The thermal stability analysis by circular dichroism (CD) of HuR₂₋₉₉ and HuR₂₋₁₈₉ revealed a single melting temperature of similar value for both protein variants (Supplementary Figure S3A). Moreover, overlapping of nuclear magnetic resonance (NMR) heteronuclear single quantum coherence (2D-¹H-¹⁵N-HSQC) experiments with HuR₂₋₉₉ and HuR₂₋₁₈₉ showed minimal chemical shift perturbation differences (Δ CSPs < 0.03 ppm) for residues located at the first domain of HuR₂₋₁₈₉ vs. HuR₂₋₉₉ (Supplementary Figure S3B). Altogether, these data proved the independence of HuR RRM1 domain and allowed us to work with the simplified construction HuR₂₋₉₉ (47).

Next, we designed a phosphomimetic version of HuR₂₋₉₉ phosphorylated at Y5 (HuR₂₋₉₉ pY5) by replacing Y5 by *p*-carboxymethyl-L-phenylalanine (*p*CMF; HuR₂₋₉₉ Y5*p*CMF), which is a non-canonical amino acid extensively used to mimic phosphorytyrosine residues due to its charge and volume (27). Specific insertion of *p*CMF at the correct position was confirmed by mass digestion (Supplementary Figure S4A). We performed a thermal stability assay by CD to characterize the mutant protein. Both HuR₂₋₉₉ wild-type protein and HuR₂₋₉₉ Y5*p*CMF mutant presented similar denaturation profiles, proving that the phosphomimetic mutant maintained the overall protein structure (Supplementary Figure S3A and S5A). Overlap between 2D-¹H-¹⁵N-HSQC spectra from HuR₂₋₉₉ wild-type and HuR₂₋₉₉ Y5*p*CMF showed almost no general differences (Δ CSPs < 0.03 ppm) (Supplementary Figure S5B and S5C).

Although the Y5 phosphorylation does not significantly alter the protein structure, 1 μ s molecular dynamics (MDs) simulations revealed dynamic changes. Simulations showed that HuR₂₋₉₉ pY5 and HuR₂₋₉₉ Y5*p*CMF contain a more dynamic N-end and β_2 - β_3 loop than HuR₂₋₉₉ wild-type (Figure 2A and Supplementary Figure S6A). The representations of the contact frequency of each residue with the others during the MDs (contact-maps) revealed differences on the contact pattern of the same regions (N-end and β_2 - β_3 loop) between the wild-type and the phosphorylated or phosphomimetic proteins (Figure 2B). More specifically, the contacts between the first N-terminal stretch and beta sheets β_1 and β_3 , observed in the wild-type model, were debilitated in HuR₂₋₉₉ pY5 or HuR₂₋₉₉ Y5*p*CMF, due to weaker interactions of the flexible N-end mapping the protein surface (Figure 2A and B).

To further study this phenomenon, we analysed the anionic distribution of HuR₂₋₉₉ wild-type and HuR₂₋₉₉ Y5*p*CMF using NMR solvent paramagnetic relaxation enhancement (sPRE) experiments. For these assays, we used a negatively charged paramagnetic probe—carboxy-PROXYL—and a neutral paramagnetic probe—carbamoyl-PROXYL (Supplementary Figure S7A). Positively charged regions of the protein attract the negative probe, thus accumulating anions (positive $\Delta\Gamma_2$ values). Conversely, the neutral probes dis-

tribute uniformly around the protein. Regions with higher rates for the neutral than for the negative probe present negative values of $\Delta\Gamma_2$, indicating anions exclusion (48). In general, HuR₂₋₉₉ Y5*p*CMF tends to exclude more anions than HuR₂₋₉₉ wild-type (Figure 2C and Supplementary Figure S7B, C). This effect is especially notable on the β_2 - β_3 loop, together with the α_1 -helix region. Thus, the negative charge of *p*CMF residue ejects the negative probe not only on its surroundings—which was expected due to the chemical nature of the modified residue—but also on the opposite side of the protein, probably due to the highly dynamic N-terminal stretch of the phosphomimetic protein, as pointed out by the MD simulations.

Y5 phosphorylation changes HuR nucleo-cytoplasmic shuttling sequence exposure

HuR possesses a nucleo-cytoplasmic shuttling (HNS) sequence, located at the hinge region between RRM2 and RRM3, that regulates its transport across the nuclear envelope (9). PTMs influencing HuR nucleo-cytoplasmic distribution are usually located in or near the hinge region (1) and, therefore, it was unexpected that a phosphorylation at the N-terminal stretch of the protein could alter its cellular localization (Figure 1). To better understand the effect of Y5 phosphorylation on full-length HuR dynamics, we performed 300 ns MD simulations with HuR full-length (HuR₁₋₃₂₆) wild-type, HuR₁₋₃₂₆ pY5 and HuR₁₋₃₂₆ Y5*p*CMF (Figure 3 and Supplementary Figure S6B and S6C). The main differences on the contact map representations correspond to the N-terminal stretch, the first domain of HuR and the hinge region (Figure 3A and Supplementary Figure S6C). Specifically, the regions of the β_2 - β_3 loop and the α_1 -helix of RRM1 establish contacts with the second half of the hinge region (residues 219–244) on the wild-type model. However, these contacts disappear on the MD simulations of the phosphorylated and phosphomimetic species, whereas novel contacts appear between the initial region of the hinge domain (residues 182–192) and the N-terminal stretch and the α_2 -helix of RRM1. On the phosphorylated protein, the beginning of the HNS sequence (residues 203–212) establishes contacts with the disordered N-terminal stretch and the α_2 -helix of RRM1. The differences on the contact pattern between HuR₁₋₃₂₆ wild-type and HuR₁₋₃₂₆ pY5 result on two differentiated areas on the hinge region according to their differences on the solvent-accessible surface area (SASA) (Figure 3B). Therefore, the first half of the hinge region, responsible for the NLS activity, is more exposed on the wild-type protein, whereas the second half is more exposed on the phosphorylated protein, enabling the shuttle of HuR to the cytoplasm (see Figure 1B).

Phosphorylation at Y5 increases HuR RRM1 oligomerization

HuR oligomerization has been previously observed in cancer cell lines, predominantly in the cytoplasm (23,49). Interestingly, when further analysing the MD and sPRE-NMR experiments, the most remarkable differences between HuR₂₋₉₉ wild-type and HuR₂₋₉₉ Y5*p*CMF correspond to the β_2 - β_3 loop and the α_1 -helix. Remarkably, these regions were previously described as responsible for the dimerization of HuR RRM1 (28).

Thus, we transfected HeLa cells with plasmids bearing V5-tagged wild-type HuR or HuR Y5F and detected them

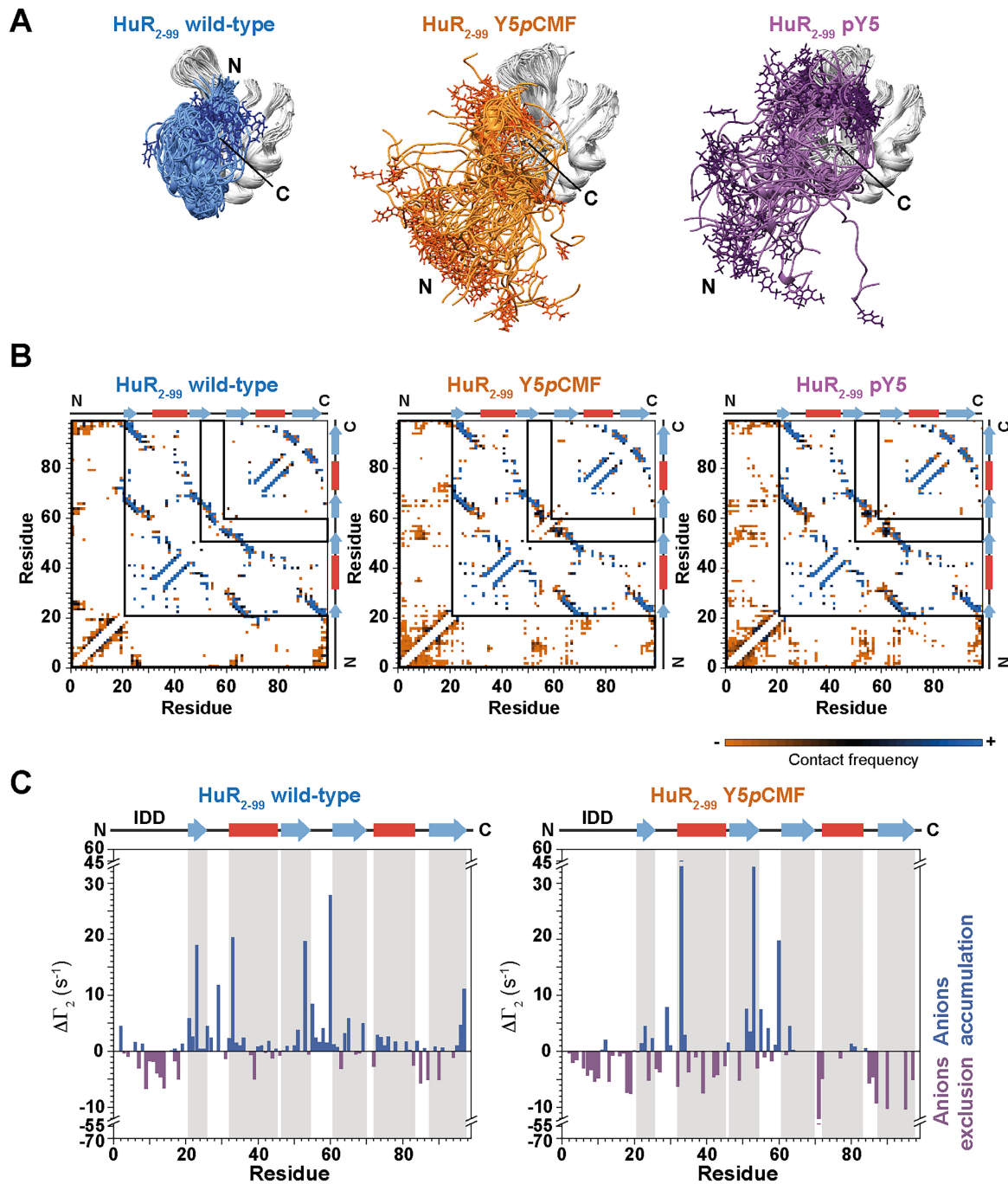


Figure 2. Y5 phosphorylation effect on HuR structure and dynamics. **(A)** Superimposition of ribbon representation of 100 structures of HuR₂₋₉₉ wild-type, HuR₂₋₉₉ Y5pCMF and HuR₂₋₉₉ pY5 during 1 μs of molecular dynamics (MDs) simulations. Residues 1–20 are colored in cyan, orange, and purple respectively. Side chain of residue 5 is represented in each structure. Residues 21–99 are in grey. **(B)** Contact maps of HuR₂₋₉₉ wild-type, Y5pCMF and pY5 from 1 μs MDs simulations. α -helices and β -sheets of HuR RRM1 are represented with red rectangles and blue arrows respectively. Black boxes indicate the regions containing the main differences between HuR₂₋₉₉ constructs. **(C)** Differences between the NMR solvent Paramagnetic Relaxation Enhancement (sPRE) Γ_2 rates for the analogous paramagnetic probes carboxy-PROXYL (negative) and carbamoyl-PROXYL (neutral) of HuR₂₋₉₉ wild-type and HuR₂₋₉₉ Y5pCMF proteins. Higher Γ_2 rates for negative probe than for neutral probe indicate anions accumulation (blue). The opposite indicates anions exclusion (pink). α -helices are represented with red rectangles and β -sheets with blue arrows. Residues in secondary structures are shaded in grey. IDD stands for intrinsically disordered domain.

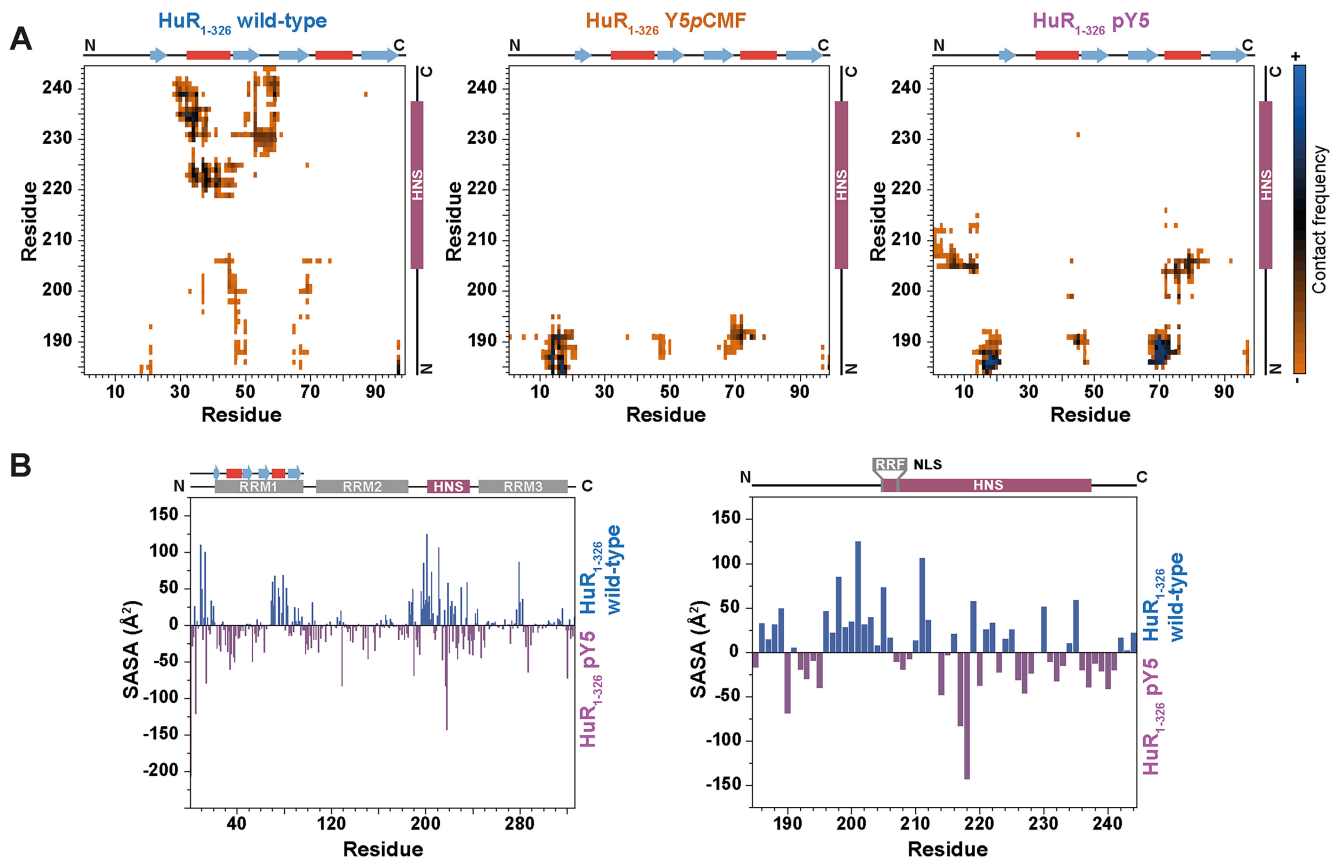


Figure 3. HuR phosphorylation at Y5 modifies HuR nucleo-cytoplasmic shuttling sequence solvent exposure. **(A)** Contact maps zooms of full length HuR (HuR₁₋₃₂₆) wild-type, Y5pCMF and pY5 from 300 ns molecular dynamics (MDs) simulations. **(B)** Differences between solvent-accessible surface area (SASA) by residues of HuR₁₋₃₂₆ wild-type and pY5 during the MDs. Residues more exposed on HuR₁₋₃₂₆ wild-type are in blue, and residues more exposed on HuR₁₋₃₂₆ pY5 are in pink. α -helices and β -sheets of HuR RRM1 are represented with red rectangles and blue arrows respectively. RRM domains are represented with grey rectangles, and HuR nucleo-cytoplasmic shuttling (HNS) sequence, with a pink rectangle. The residues implicated on the nuclear localization signal (NLS) activity are indicated in the right panel.

by western-blot in non-reducing and non-denaturing conditions, comparing with reducing and denaturing conditions, using V5 antibody (Figure 4A). Importantly, although bands corresponding to monomeric or dimeric HuR were present in both samples at the same intensity in non-reducing and non-denaturing conditions, a band corresponding to a trimer was barely present in the Y5F mutant (0.3-fold the intensity presented in the WT version). Notably, bands corresponding to dimeric and trimeric HuR disappeared in reducing and denaturing conditions. Collectively, these results demonstrate that HuR phosphorylated in Y5 exhibits a tendency for oligomerization.

Furthermore, we verified the oligomerization of both proteins *in vitro* by isothermal titration calorimetry (ITC) dilution assays (Figure 4B). In these experiments, a concentrated sample of HuR (700 μ M) is titrated into the cell containing buffer, thus diluting the protein, and promoting dimer dissociation. According to the analysis of ITC dilution assays, the equilibrium dissociation constant (K_D) of HuR₂₋₉₉ Y5pCMF is one order of magnitude lower than that for HuR₂₋₉₉ wild-type, indicating a higher tendency of HuR₂₋₉₉ to dimerize when it is phosphorylated at Y5. Thus, the phosphorylation of Y5 seems to play a dual role: disturb the contacts between the RRM1 β_2 - β_3 loop and the HNS sequence, and thereby promote both HuR shuttling to the cytoplasm and oligomerization.

Y5 phosphorylation modulates HuR nucleic acids interaction

Since HuR RRM1 is the principal domain involved in RNA recognition (8), we decided to study whether HuR binding to nucleic acids is affected by Y5 phosphorylation. For this purpose, we designed a recombinant full-length HuR (HuR₁₋₃₂₆, see Supplementary Figure S2C), and its phosphomimetic version by replacing Y5 by pCMF (HuR₁₋₃₂₆ Y5pCMF). The non-canonical amino acid insertion was confirmed by mass digestion (Supplementary Figure S4B). Then, we performed bio-layer interferometry (BLI) assays using a biotinylated DNA oligonucleotide of 17 bases length (17mer) and HuR₁₋₃₂₆ wild-type or HuR₁₋₃₂₆ Y5pCMF (Figure 5A). We performed similar experiments using a biotinylated DNA oligonucleotide of 7 bases (7mer) and HuR₂₋₉₉ wild-type or HuR₂₋₉₉ Y5pCMF (Supplementary Figure S8A). Given that HuR binds to adenosine and uridine-rich elements (AREs) with high affinity (50), both oligonucleotides were composed of adenine and thymine (5'-ATTTTATTTTATTTT-3' and 5'-ATTTTA-3'). Analysis of BLI experiments revealed a slightly higher nucleic acids affinity for the wild-type protein than for the phosphomimetic mutant, both for HuR₂₋₉₉ and for the full-length protein. Calorimetry assays and 2D-¹H-¹⁵N-HSQC NMR titrations with HuR₂₋₉₉ wild-type or HuR₂₋₉₉ Y5pCMF proteins and the 7mer oligonucleotide further corroborated the modest change

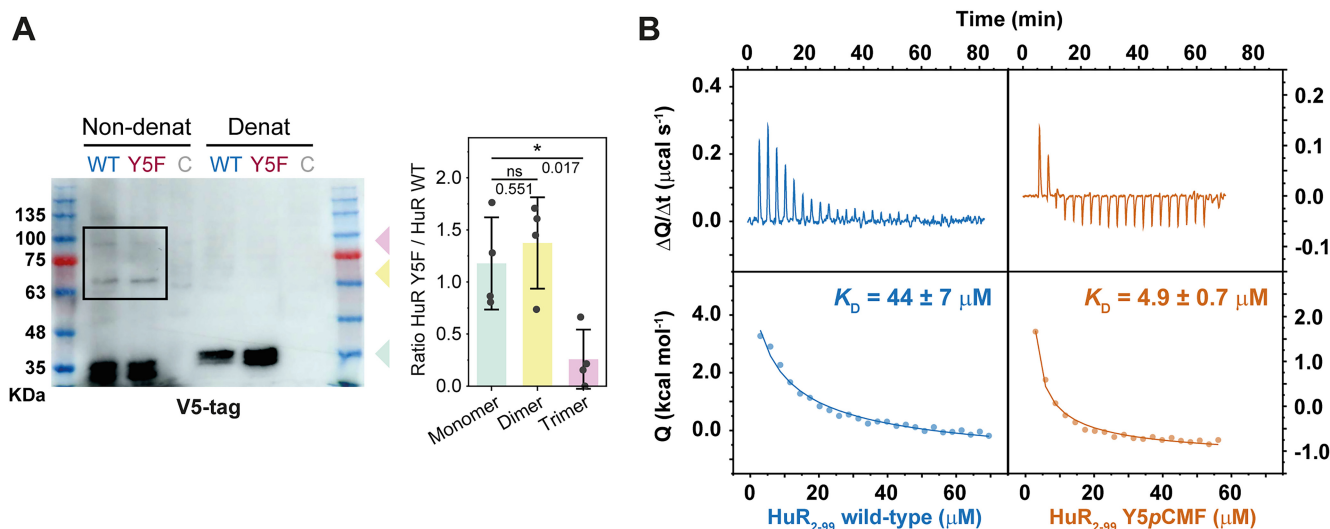


Figure 4. Y5 phosphorylation increases RRM1-dependent oligomerization of HuR. **(A)** Western-blot analysis of V5-tagged HuR versions. HeLa cells were transfected with plasmids expressing HuR-V5 or HuR Y5F-V5 variants, and subjected to analysis to detect V5-tag. Non-transfected HeLa cells were used as control (C). For samples in non-reduced and non-denatured conditions (Non-denat), reducing agents were not added and samples were not heated before loading in the SDS-PAGE gel. Arrows indicate theoretical weights for HuR monomers, dimers and trimers. The western blot showed is representative of four similar experiments. *Right panel:* Quantification of the intensities from discrete bands for HuR monomers, dimers and trimers using anti-V5-tag antibody. The average of 4 experiments is shown. Whiskers indicate standard deviation values. The significance of differences was tested using the Student's *t* test. **(B)** ITC analysis of HuR₂₋₉₉ wild-type (cyan) and HuR₂₋₉₉ Y5pCMF (orange) dilution assays. Thermograms and dissociation isotherms are shown in the *upper* and *lower* panels, respectively.

in binding affinity of the phosphomimetic protein towards nucleic acids (Figure 5B and Supplementary Figure S8B).

Surface mapping of the residues exhibiting highest Δ CSPs delimits the DNA binding interface on the β -strands of HuR RRM1 (Figure 5C and Supplementary Figure S8C–F), as already demonstrated before (28). No remarkable changes were observed between the interaction interfaces of HuR₂₋₉₉ wild-type and HuR₂₋₉₉ Y5pCMF; actually, only one residue (A96) shows a Δ CSP slightly higher for the phosphomimetic protein than for the wild-type. Nevertheless, 2D ^1H - ^{15}N -HSQC backbone conventional experiments were not able to detect hydrogen bonds involving side chains, which have a key role in HuR nucleic acid binding (6). For that reason, we performed heteronuclear in-phase single quantum coherence spectroscopy (HISQC) experiments, which takes advantage of tailored pulse sequences to analyze the ^1H - ^{15}N correlation of lysine side-chain amino groups. This method is particularly useful to study interaction dynamics between HuR and DNA, since HuR₂₋₉₉ contains five lysine residues, all of them exposed to the solvent. Additional experiments were performed to assign signals in HISQC spectra: 2D (H2C)N(CCH)-TOCSY—to detect $^{15}\text{N}\zeta$ correlations with ^1H Lys—and 2D H2CN—to monitor changes of $^1\text{H}\epsilon$ - $^{15}\text{N}\zeta$ resonance signals across temperature—(Supplementary Figure S9). Upon DNA binding, the NH_3^+ groups from lysine side chains are less susceptible to exchange with bulk H^+ (lower water-exchange rates), thus allowing their detection by NMR. 2D- ^1H - ^{15}N -HISQC titrations were carried out with HuR₂₋₉₉ wild-type or Y5pCMF and the 7mer oligonucleotide (Figure 5D). Four $-\text{NH}_3^+$ signals appeared in the free HuR₂₋₉₉ spectrum, whereas the spectra recorded at higher protein:DNA ratios (1:0.8 and 1:1.3) revealed an additional $-\text{NH}_3^+$ signal, which corresponds to K50. The resonances of lysine residues at the DNA binding interface, namely K50, K55 and K92, experienced significant chemical shifts, while the resonances of K72 and K89 signals barely moved upon DNA addition. Most importantly,

the lower signal intensity of K50, K55 and K92, which are likely the residues with a major involvement in DNA binding, for HuR₂₋₉₉ Y5pCMF mutant suggests a reduction in DNA-affinity in the phosphomimetic mutant. Altogether, these observations support that phosphorylation of Y5 only has a modest impact on nucleic acids interaction.

Nevertheless, we tested the capacity of Y5 phosphorylated HuR to interact with target mRNAs in the cell by RIP (ribonucleoprotein immunoprecipitation) analysis. For that, we transfected HeLa cells with plasmids expressing HuR-V5 or HuR Y5F-V5. After immunoprecipitation with anti-V5, the levels of specific mRNAs were measured by reverse transcription followed by real-time quantitative PCR analysis (Figure 5E). Surprisingly, the concentration of ribonucleoprotein (RNP) complexes of HuR with prothymosin alpha (PTMA) mRNA, which is a known target of HuR, increased after doxorubicin treatment. Significantly, this change was not observed for HuR Y5F. Thus, Y5 phosphorylation might affect the binding of HuR with certain mRNA targets in the cell.

Discussion

The RBP HuR is essential on vital processes, from development to cell survival upon stress conditions (51). Thus, HuR is involved in numerous diseases with diverse aetiologies, and the interest on this protein is still increasing since its discovery in 1996 (2,7,52). The activation of HuR is related to its translocation from the nucleus to the cytoplasm to play its main function, namely RNA stabilization, under diverse stimuli, for instance, DNA damage response (7,53,54). Specifically, doxorubicin was previously shown to induce HuR phosphorylation by PKC kinase, which leads to its cytoplasmic redistribution (46,55). Furthermore, the cytoplasmic fraction of HuR is more susceptible to oligomerize (23,24). However, the mechanistic details on HuR transport between nucleus and cytoplasm have not been fully elucidated and neither of the

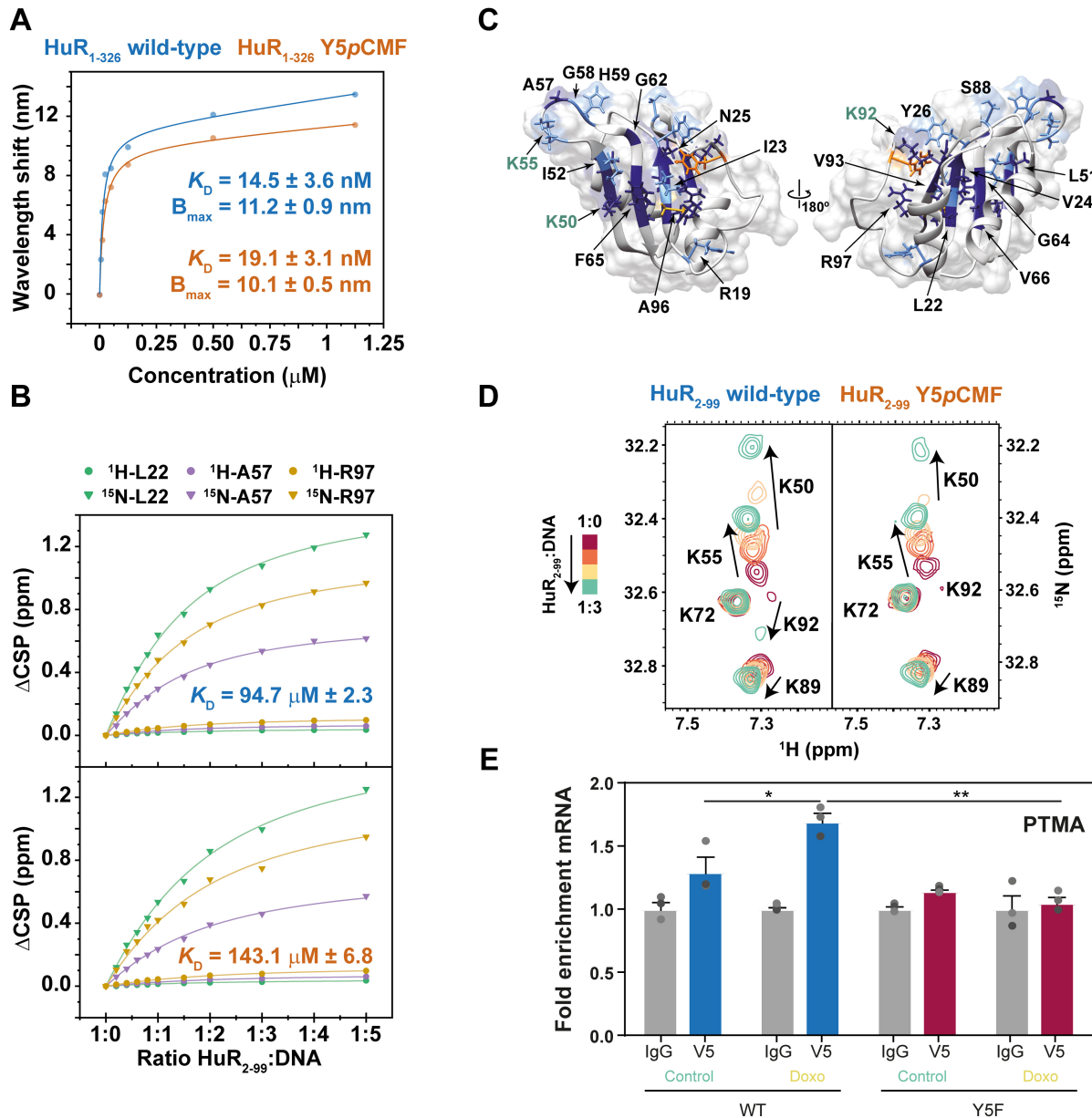


Figure 5. Phosphorylation at HuR Y5 regulates HuR nucleic acids affinity. **(A)** Biolayer Interferometry (BLI) binding analysis of full length HuR (HuR₁₋₃₂₆) wild-type (cyan) and Y5pCMF mutant (orange) with a 17mer DNA-oligonucleotide (5'-ATTTTATTTTATTTT-3'). **(B)** Curves representing the best global fit of NMR CSPs for several amide signals in the indirect (15 N) and direct (1 H) dimensions, at a 1:5 ratio (protein:DNA), for HuR₂₋₉₉ wild-type (upper panel) and Y5pCMF mutant (lower panel). **(C)** Ribbon and surface map of HuR₂₋₉₉ wild-type. Residues exhibiting CSPs higher than twice the standard deviation (2σ) for HuR₂₋₉₉ wild-type and HuR₂₋₉₉ Y5pCMF are represented by dark blue and those ones with values between 1σ and 2σ , in cyan. K96, which is significantly affected only in HuR₂₋₉₉ Y5pCMF mutant, is colored by yellow. Y5 is colored in orange. Side chains of the residues with CSPs higher than 1σ are shown. PDB ID: 5SZW (28). **(D)** Superimposed 2D 1 H- 15 N HSQC titration spectra of 15 N-labeled HuR₂₋₉₉ wild-type (left panel) and Y5pCMF mutant (right panel) up to a ratio 1:3 (protein:DNA). **(E)** HeLa cells were transfected with HuR-V5 or HuR Y5F-V5, and treated in the absence or presence of 10 μ M doxorubicin for 4 h. Ribonucleoprotein immunoprecipitation (RIP) analysis was used to measure the interaction between HuR variants and prothymosin alpha (PTMA) mRNA. GAPDH mRNA was measured for normalization, and data are represented as enrichment of the mRNAs in V5 IP samples relative to the levels in IgG IP samples. The graphs represent the mean and standard deviation from three independent experiments.

numerous PTMs regulating HuR seem to control its oligomerization (1,2,5,56). In this study, we describe a new pathway for HuR activation elicited by DNA damage response which involves phosphorylation at Y5 for the first time. We have confirmed Y5 phosphorylation in cancer cell models, i.e. HeLa and Jurkat cells (Figure 1). This PTM not only promotes HuR cytoplasmic accumulation, but also protein oligomerization.

Previous studies determined the proximity between HuR RRM1 and RRM3 by PRE-NMR experiments (8). Specifi-

cally, the spin-labelled-C245 of RRM3 is close to the β_2 - β_3 loop and the helical region of RRM1. In the same report, 2D- 1 H- 15 N-HSQC experiments were also performed with HuR RRM1-2, HuR RRM1-3 and a version of HuR RRM1-3 where the hinge region is mutated by repetitions of Gly-Gly-Ser. Relevant Δ CSPs at the β_2 - β_3 loop of RRM1 were found when comparing the spectrum of HuR RRM1-2 with that of HuR RRM1-3, indicating a change in the chemical environment of the β_2 - β_3 loop of RRM1 in the presence of the RRM3

domain. However, the analysis with the mutated version of HuR RRM1-3 revealed no significant Δ CSPs in that region (8). This difference on Δ CSPs, dependent on the nature of the hinge region, confirms its closeness to RRM1 in the context of the full-length protein.

Although Y5 phosphorylation occurs at the N-terminal disordered region, our data support that this modification increases the dynamics of the hinge region and modifies its contacts with the first domain of HuR (Figure 3A). These changes alter the solvent exposure of the HNS sequence. According to our MDs simulations, the hinge domain can be divided in two regions (Figure 3B). Whereas the second half of the hinge region is buried in the non-modified protein, the residues with NLS activity in the first half are exposed. Thus, it is likely that the different solvent exposure in this region contributes to the different subcellular localization observed for the phosphorylated protein (Figure 1).

On the other hand, our MDs simulations and sPRE-NMR experiments indicate that the solvent exposure of the first domain also changes when HuR is phosphorylated at Y5 (Figure 2). Specifically, the contacts of the hinge region with the α_1 -helix and the β_2 - β_3 loop disappear. Calorimetry assays indicate that their exposure suppose a 10-fold reduction in dimerization K_D , which will trigger an increase in HuR RRM1 dimeric population (Figure 4B). Although non-modified HuR dimerizes exclusively through RRM3 domain in the context of the full-length protein (8,57,58), studies performed with isolated domain RRM1 revealed the ability of this domain to form dimers in a Cys-independent manner (28). In fact, we confirmed that HuR phosphorylated in Y5 presents a tendency for oligomerization in HeLa cells (Figure 4A). Thus, we propose that full-length HuR needs to be phosphorylated at Y5 to release α_1 -helix and the β_2 - β_3 loop, and permit oligomerization mediated by RRM1.

We also tested the effect of Y5 phosphorylation on HuR-nucleic acids binding. Dissociation constant of phosphomimetic HuR is slightly higher than for the non-modified protein. A possible explanation for this faint difference is the repulsion generated between the negatively charged nucleic acids and pCMF or pY amino acids. Moreover, the N-end of HuR establishes numerous transient contacts with RRM1 β -sheets when Y5 is phosphorylated, possibly sterically hindering its interaction with nucleic acids (Figure 2). Therefore, although Y5 phosphorylation is not directly involved on the control of HuR-RNA binding, the extra negative charge might lead to a reduction in the binding capacity of the protein. While HuR dimerization through RRM3 increases RNA binding *in vitro*, it seems to play an autoinhibitory role in the cell, reducing the mRNA stabilization activity of HuR (59). The slightly reduced interaction with DNA observed for HuR Y5pCMF could alternatively be due to a negative effect of dimerization. Indeed, RRM1 dimerization is reduced by nucleic acid binding in the non-modified protein (28). Nonetheless, Y5 phosphorylation seems to exert an effect in the interaction with HuR specific mRNA targets, such as PTMA, demonstrating a physiological role of this post-translational modification.

In summary, we present a new phosphorylation site at the intrinsically disordered N-end of HuR that increases the dynamics of the hinge-region and modifies the solvent exposure of the HNS sequence. Thus, the phosphorylation at Y5 interferes with HuR shuttling between nucleus and cytoplasm, resulting on the cytoplasmic accumulation of HuR. In addition, this PTM is responsible for HuR oligomerization by its

first domain upon the release of the implicated residues. Moreover, the detection of phosphorylated HuR at Y5 in cancer cell models (HeLa and Jurkat cells) highlights the possible implications of Y5 phosphorylation in cancer. As a new activation pathway of HuR, phosphorylation at Y5 opens a study field on the regulation of this protein, and it contributes to the understanding of HuR function.

Data availability

The data underlying this article are available in the article and in its online supplementary material or will be shared on reasonable request to the corresponding author. The assignment data are available in BMRB and can be accessed with 52173 deposition number.

Supplementary data

Supplementary Data are available at NAR Online.

Acknowledgements

Authors acknowledge Prof. M. Gorospe for the kind gift of the plasmid encoding HuR, Prof. P. Celie for the kinase domain of JAK3, and Prof. J. M. Lassaletta for his help with pCMF synthesis. The authors wish to thank Dr. Alejandro Velázquez-Cruz for critical reading of the manuscript and technical advice, Mr. Marc Herrmann for excellent technical assistance, and Dr. Francisco Rivero-Rodríguez and Dr. Sofía M. García-Mauriño for their support with NMR assignment and kinase assays. We also thank the staff at the NMR facilities at the Scientific and Technological centres of the University of Barcelona (CCiTUB, 21_R-LRB14), the NMR facility at the Research, Technology and Innovation centre of the University of Seville (CITIUS), and the BIO-MS laboratory (UPO), the microscopy, chromatography, imaging and centrifuges services at the Institute of Plant Biochemistry and Photosynthesis (IBVF), and the Biomolecular Interaction Platform (cicCartuja, Seville).

Author contributions: B.B.J.: Conceptualization, Data curation, Formal analysis, Investigation, Methodology, Visualization, Writing—original draft. L.C.G.: Conceptualization, Data curation, Formal analysis, Investigation, Methodology, Project administration, Supervision, Writing—original draft. G.P.M.: Conceptualization, Formal analysis, Methodology, Writing—review & editing. C.M.R.G.: Investigation, Formal analysis, Writing—original draft. A.V.C.: Formal analysis, Writing—review & editing. L.A.M.C.: Conceptualization, Writing—review & editing. M.A.R.: Conceptualization, Funding acquisition, Resources, Writing—review & editing. I.D.M.: Conceptualization, Data curation, Funding acquisition, Methodology, Project administration, Resources, Supervision, Writing—original draft.

Funding

Work supported by the Agencia Estatal de Investigación (AEI), Spanish Ministry of Science and Innovation (MCIN) and ‘ERDF A way of making Europe’ [MCIN/AEI/10.13039/501100011033, grant numbers PID2021-126663NB-I00 and PID2020-117116RP]; Andalusian Government [P18-FR-3487, and postdoctoral contract PAIDI-Doctor 2020 DOC_00796 to L.C.G.]; Spanish Min-

istry of Education, Culture and Sport [FPU17/04604 to G.P.M.]; C.M.R.G. was supported by a postdoctoral contract Margarita Salas (University of Extremadura) from the Program of Requalification of the Spanish University System (Spanish Ministry of Universities) financed by the European Union – NextGenerationEU. Funding for open access charge: Universidad de Sevilla (Biblioteca Universidad de Sevilla) has an agreement with Oxford University Press, including the 100% cover of Open Access Publication in *Nucleic Acids Research*.

Conflict of interest statement

None declared.

References

- Grammatikakis,I., Abdelmohsen,K. and Gorospe,M. (2017) Posttranslational control of HuR function. *Wiley Interdiscipl. Rev.: RNA*, **8**, <https://doi.org/10.1002/wrna.1372>.
- Velázquez-Cruz,A., Baños-Jaime,B., Díaz-Quintana,A., De la Rosa,M.A. and Díaz-Moreno,I. (2021) Post-translational control of RNA-binding proteins and disease-related dysregulation. *Front. Mol. Biosci.*, **8**, 658852.
- Battaglia-Hsu,S.F., Ghemrawi,R., Coelho,D., Dreumont,N., Mosca,P., Hergalant,S., Gauchotte,G., Sequeira,J.M., Ndiongue,M., Houlgatte,R., *et al.* (2018) Inherited disorders of cobalamin metabolism disrupt nucleocytoplasmic transport of mRNA through impaired methylation/phosphorylation of ELAVL1/HuR. *Nucleic Acids Res.*, **46**, 7844–7857.
- Brennan,C.M., Gallouzi,I.E. and Steitz,J.A. (2000) Protein ligands to HuR modulate its interaction with target mRNAs in vivo. *J. Cell Biol.*, **151**, 1–14.
- Gallouzi,I.E., Brennan,C.M. and Steitz,J.A. (2001) Protein ligands mediate the CRM1-dependent export of HuR in response to heat shock. *RNA*, **7**, 1348–1361.
- Wang,H., Zeng,F., Liu,Q., Liu,H., Liu,Z., Niu,L., Teng,M. and Li,X. (2013) The structure of the ARE-binding domains of Hu antigen R (HuR) undergoes conformational changes during RNA binding. *Acta Crystallogr. Sect. D Biol. Crystallogr.*, **69**, 373–380.
- Lachiondo-Ortega,S., Delgado,T.C., Baños-Jaime,B., Velázquez-Cruz,A., Díaz-Moreno,I. and Martínez-Chantar,M.L. (2022) Hu Antigen R (HuR) protein structure, function and regulation in hepatobiliary tumors. *Cancers*, **14**, 2666.
- Pabis,M., Popowicz,G.M., Stehle,R., Fernández-Ramos,D., Asami,S., Warner,L., García-Mauriño,S.M., Schlundt,A., Martínez-Chantar,M.L., Díaz-Moreno,I., *et al.* (2019) HuR biological function involves RRM3-mediated dimerization and RNA binding by all three RRMs. *Nucleic Acids Res.*, **47**, 1011–1029.
- Fan,X.C. and Steitz,J.A. (1998) HNS, a nuclear-cytoplasmic shuttling sequence in HuR. *Proc. Nat. Acad. Sci. U.S.A.*, **95**, 15293–15298.
- Ke,Y., Lv,X., Fu,X., Zhang,J., Bohio,A.A., Zeng,X., Hao,W., Wang,R., Boldogh,I. and Ba,X. (2021) Poly(ADP-ribosylation) enhances HuR oligomerization and contributes to pro-inflammatory gene mRNA stabilization. *Cell. Mol. Life Sci.*, **78**, 1817–1835.
- Beauchamp,P., Nassif,C., Hillock,S., Van Der Giessen,K., Von Roretz,C., Jasmin,B.J. and Gallouzi,I.E. (2010) The cleavage of HuR interferes with its transportin-2-mediated nuclear import and promotes muscle fiber formation. *Cell Death Differ.*, **17**, 1588–1599.
- Von Roretz,C., Beauchamp,P., Di Marco,S. and Gallouzi,I.E. (2011) HuR and myogenesis: being in the right place at the right time. *Biochim. Biophys. Acta - Mol. Cell Res.*, **1813**, 1663–1667.
- Güttinger,S., Mühlhäusser,P., Koller-Eichhorn,R., Brennecke,J. and Kutay,U. (2004) Transportin2 functions as importin and mediates nuclear import of HuR. *Proc. Nat. Acad. Sci. U.S.A.*, **101**, 2918–2923.
- Doller,A., Huwiler,A., Müller,R., Radeke,H.H., Pfeilschifter,J. and Eberhardt,W. (2007) Protein kinase C α -dependent phosphorylation of the mRNA-stabilizing factor HuR: Implications for posttranscriptional regulation of cyclooxygenase-2. *Mol. Biol. Cell*, **18**, 2137–2148.
- Doller,A., Schlepckow,K., Schwalbe,H., Pfeilschifter,J. and Eberhardt,W. (2010) Tandem phosphorylation of serines 221 and 318 by protein kinase C δ coordinates mRNA binding and nucleocytoplasmic shuttling of HuR. *Mol. Cell. Biol.*, **30**, 1397–1410.
- Yoon,J.H., Abdelmohsen,K., Srikantan,S., Guo,R., Yang,X., Martindale,J.L. and Gorospe,M. (2014) Tyrosine phosphorylation of HuR by JAK3 triggers dissociation and degradation of HuR target mRNAs. *Nucleic Acids Res.*, **42**, 1196–1208.
- Filippova,N., Yang,X. and Nabors,L.B. (2015) Growth factor dependent regulation of centrosome function and genomic instability by HuR. *Biomolecules*, **5**, 263–281.
- Fan,X.C. and Steitz,J.A. (1998) Overexpression of HuR, a nuclear-cytoplasmic shuttling protein, increases the in vivo stability of ARE-containing mRNAs. *EMBO J.*, **17**, 3448–3460.
- Bonomo,I., Assoni,G., Pietra,V.L., Canarutto,G., Facen,E., Donati,G., Zucal,C., Genovese,S., Micaelli,M., Pérez-Rafols,A., *et al.* (2023) HuR modulation counteracts lipopolysaccharide response in murine macrophages. *Dis. Models Mech.*, **16**, dmm050120.
- Scheiba,R.M., Aroca,Á. and Díaz-Moreno,I. (2012) HuR thermal stability is dependent on domain binding and upon phosphorylation. *Eur. Biophys. J.*, **41**, 597–605.
- Bhargava,P. and Schnellmann,R.G. (2017) Mitochondrial energetics in the kidney. *Nat. Rev. Nephrol.*, **13**, 629–646.
- Schultz,C.W., Preet,R., Dhir,T., Dixon,D.A. and Brody,J.R. (2020) Understanding and targeting the disease-related RNA binding protein human antigen R (HuR). *Wiley Interdiscipl. Rev.: RNA*, **11**, e1581.
- Filippova,N., Yang,X., Ananthan,S., Sorochinsky,A., Hackney,J.R., Gentry,Z., Bae,S., King,P. and Nabors,L.B. (2017) Hu antigen R (HuR) multimerization contributes to glioma disease progression. *J. Biol. Chem.*, **292**, 16999–17010.
- Meisner,N.C., Hintersteiner,M., Mueller,K., Bauer,R., Seifert,J.M., Naegeli,H.U., Ottl,J., Oberer,L., Guenat,C., Moss,S., *et al.* (2007) Identification and mechanistic characterization of low-molecular-weight inhibitors for HuR. *Nat. Chem. Biol.*, **3**, 508–515.
- Schindelin,J., Arganda-Carreras,I., Frise,E., Kaynig,V., Longair,M., Pietzsch,T., Preibisch,S., Rueden,C., Saalfeld,S., Schmid,B., *et al.* (2012) Fiji: An open-source platform for biological-image analysis. *Nat. Methods*, **9**, 676–682.
- Yoon,J.H., Abdelmohsen,K., Srikantan,S., Guo,R., Yang,X., Martindale,J.L. and Gorospe,M. (2014) Tyrosine phosphorylation of HuR by JAK3 triggers dissociation and degradation of HuR target mRNAs. *Nucleic. Acids. Res.*, **42**, 1196–1208.
- Pérez-Mejías,G., Velázquez-Cruz,A., Guerra-Castellano,A., Baños-Jaime,B., Díaz-Quintana,A., González-Arzoila,K., Ángel De la Rosa,M. and Díaz-Moreno,I. (2020) Exploring protein phosphorylation by combining computational approaches and biochemical methods. *Comput. Struct. Biotechnol. J.*, **18**, 1852–1863.
- Lixa,C., Mujo,A., de Magalhães,M.T.Q., Almeida,F.C.L., Lima,L.M.T.R. and Pinheiro,A.S. (2018) Oligomeric transition and dynamics of RNA binding by the HuR RRM1 domain in solution. *J. Biomol. NMR*, **72**, 179–192.
- Webb,B. and Sali,A. (2017) Protein structure modeling with MODELLER. *Methods Mol. Biol.*, **1654**, 39–54.
- Homeyer,N., Horn,A.H.C., Lanig,H. and Sticht,H. (2006) AMBER force-field parameters for phosphorylated amino acids in different protonation states: phosphoserine, phosphothreonine, phosphotyrosine, and phosphohistidine. *J. Mol. Model.*, **12**, 281–289.

31. Guerra-Castellano, A., Díaz-Quintana, A., Moreno-Beltrán, B., López-Prados, J., Nieto, P.M., Meister, W., Staffa, J., Teixeira, M., Hildebrandt, P., De La Rosa, M.A., *et al.* (2015) Mimicking tyrosine phosphorylation in human cytochrome c by the evolved tRNA synthetase technique. *Chem. Eur. J.*, **21**, 15004–15012.
32. Case, D.A., Belfon, K., Ben-Shalom, I.Y., Brozell, S.R., Cerutti, D.S., Cheatham, T.E. III, Cruzeiro, V.W.D., Darden, T.A., Duke, R.E., *et al.* (2020) AMBER 2020.
33. Eastman, P., Swails, J., Chodera, J.D., McGibbon, R.T., Zhao, Y., Beauchamp, K.A., Wang, L.P., Simmonett, A.C., Harrigan, M.P., Stern, C.D., *et al.* (2017) OpenMM 7: Rapid development of high performance algorithms for molecular dynamics. *PLoS Comput. Biol.*, **13**, e1005659.
34. Maier, J.A., Martinez, C., Kasavajhala, K., Wickstrom, L., Hauser, K.E. and Simmerling, C. (2015) ff14SB: Improving the accuracy of protein side chain and backbone parameters from ff99SB. *J. Chem. Theory Comput.*, **11**, 3696–3713.
35. Izadi, S., Anandakrishnan, R. and Onufriev, A.V. (2014) Building water models: A different approach. *J. Phys. Chem. Lett.*, **5**, 3863–3871.
36. Roe, D.R. and Cheatham, T.E. (2013) PTRAJ and CPPTRAJ: Software for processing and analysis of molecular dynamics trajectory data. *J. Chem. Theory Comput.*, **9**, 3084–3095.
37. McGibbon, R.T., Beauchamp, K.A., Harrigan, M.P., Klein, C., Swails, J.M., Hernández, C.X., Schwantes, C.R., Wang, L.P., Lane, T.J. and Pande, V.S. (2015) MDTraj: a modern open library for the analysis of molecular dynamics trajectories. *Biophys. J.*, **109**, 1528–1532.
38. Iwahara, J., Tang, C. and Marius Clore, G. (2007) Practical aspects of 1H transverse paramagnetic relaxation enhancement measurements on macromolecules. *J. Magn. Reson.*, **184**, 185–195.
39. Moreno-Beltrán, B., Díaz-Quintana, A., González-Arzo, K., Velázquez-Campoy, A., De La Rosa, M.A. and Díaz-Moreno, I. (2014) Cytochrome c1 exhibits two binding sites for cytochrome c in plants. *Biochim. Biophys. Acta - Bioenerget.*, **1837**, 1717–1729.
40. Lee, W., Tonelli, M. and Markley, J.L. (2015) NMRFAM-SPARKY: enhanced software for biomolecular NMR spectroscopy. *Bioinformatics*, **31**, 1325–1327.
41. Pettersen, E.F., Goddard, T.D., Huang, C.C., Couch, G.S., Greenblatt, D.M., Meng, E.C. and Ferrin, T.E. (2004) UCSF Chimera - A visualization system for exploratory research and analysis. *J. Comput. Chem.*, **25**, 1605–1612.
42. Sharma, K., D'Souza, R.C.J., Tyanova, S., Schaab, C., Wiśniewski, J.R., Cox, J. and Mann, M. (2014) Ultradeep human phosphoproteome reveals a distinct regulatory nature of Tyr and Ser/Thr-based signaling. *Cell Rep.*, **8**, 1583–1594.
43. Huang, H., Petersen, M.H., Ibañez-Vea, M., Lassen, P.S., Larsen, M.R. and Palmisano, G. (2016) Simultaneous enrichment of cysteinecontaining peptides and phosphopeptides using a cysteine-specific phosphonate adaptable tag (CysPAT) in combination with titanium dioxide (TiO₂) chromatography. *Mol. Cell. Proteomics*, **15**, 3282–3296.
44. David, P.S., Tanveer, R. and Port, J.D. (2007) FRET-detectable interactions between the ARE binding proteins, HuR and p37AUF1. *RNA*, **13**, 1453–1468.
45. Kedersha, N., Cho, M.R., Li, W., Yacono, P.W., Chen, S., Gilks, N., Golan, D.E. and Anderson, P. (2000) Dynamic shuttling of TIA-1 accompanies the recruitment of mRNA to mammalian stress granules. *J. Cell Biol.*, **151**, 1257–1268.
46. Latorre, E., Tebaldi, T., Viero, G., Spartà, A.M., Quattrone, A. and Provenzano, A. (2012) Downregulation of HuR as a new mechanism of doxorubicin resistance in breast cancer cells. *Mol. Cancer*, **11**, 13.
47. Díaz-Moreno, I., Hollingworth, D., Kelly, G., Martin, S., García-Mayoral, M.F., Briata, P., Gherzi, R. and Ramos, A. (2010) Orientation of the central domains of KSRP and its implications for the interaction with the RNA targets. *Nucleic. Acids. Res.*, **38**, 5193–5205.
48. Yu, B. and Iwahara, J. (2021) Experimental approaches for investigating ion atmospheres around nucleic acids and proteins. *Comput. Struct. Biotechnol. J.*, **19**, 2279–2285.
49. Chu, P.C., Chuang, H.C., Kulp, S.K. and Chen, C.S. (2012) The mRNA-stabilizing factor HuR protein is targeted by β -TrCP protein for degradation in response to glycolysis inhibition. *J. Biol. Chem.*, **287**, 43639–43650.
50. Eberhardt, W., Doller, A., Akool, E.S. and Pfeilschifter, J. (2007) Modulation of mRNA stability as a novel therapeutic approach. *Pharmacol. Ther.*, **114**, 56–73.
51. Pacwa, A., Machowicz, J., Akhtar, S., Rodak, P., Liu, X., Pietrucha-Dutczak, M., Lewin-Kowalik, J., Amadio, M. and Smedowski, A. (2023) Deficiency of the RNA-binding protein ELAVL1/HuR leads to the failure of endogenous and exogenous neuroprotection of retinal ganglion cells. *Front. Cell. Neurosci.*, **17**, 1131356.
52. Ma, W.J., Cheng, S., Campbell, C., Wright, A. and Furneaux, H. (1996) Cloning and characterization of HuR, a ubiquitously expressed Elav-like protein. *J. Biol. Chem.*, **271**, 8144–8151.
53. Kim, H.H., Abdelmohsen, K. and Gorospe, M. (2010) Regulation of HuR by DNA damage response Kinases. *J. Nucleic Acids*, **2010**, 981487.
54. Hashimoto, M., Tsugawa, T., Kawagishi, H., Asai, A. and Sugimoto, M. (2014) Loss of HuR leads to senescence-like cytokine induction in rodent fibroblasts by activating NF- κ B. *Biochim. Biophys. Acta - Gen. Subj.*, **1840**, 3079–3087.
55. Latorre, E., Castiglioni, I., Gatto, P., Carelli, S., Quattrone, A. and Provenzano, A. (2014) Loss of protein kinase C δ /HuR interaction is necessary to doxorubicin resistance in breast cancer cell lines. *J. Pharmacol. Exp. Ther.*, **349**, 99–106.
56. Rebane, A., Aab, A. and Steitz, J.A. (2004) Transportins 1 and 2 are redundant nuclear import factors for hnRNP A1 and HuR. *RNA*, **10**, 590–599.
57. Díaz-Quintana, A., García-Mauriño, S.M. and Díaz-Moreno, I. (2015) Dimerization model of the C-terminal RNA Recognition Motif of HuR. *FEBS Lett.*, **589**, 1059–1066.
58. Scheiba, R.M., De Opakua, A.I., Díaz-Quintana, A., Cruz-Gallardo, I., Martínez-Cruz, L.A., Martínez-Chantar, M.L., Blanco, F.J. and Díaz-Moreno, I. (2014) The C-terminal RNA binding motif of HuR is a multi-functional domain leading to HuR oligomerization and binding to U-rich RNA targets. *RNA Biol.*, **11**, 1250–1261.
59. Ripin, N., Boudet, J., Duszczyn, M.M., Hinniger, A., Faller, M., Krepl, M., Gadi, A., Schneider, R.J., Sponer, J., Meisner-Kober, N.C., *et al.* (2019) Molecular basis for AU-rich element recognition and dimerization by the HuR C-terminal RRM. *Proc. Nat. Acad. Sci. U.S.A.*, **116**, 2935–2944.